Journal of Dynamic Systems, Measurement and Control. Received December 18, 2014;
Accepted manuscript posted June 2, 2015. doi:10.1115/1.4030723

Simultaneous Optimization of Damping and Tracking Controller Parameters via Selective Pole Placement for Enhanced Positioning Bandwidth of Nanopositioners

Douglas Russell
School of Engineering
University of Aberdeen
UK
Email: r01dr12@abdn.ac.uk

Andrew J. Fleming
Centre for Complex Dynamic Systems and Control
School of Electrical Engineering and Computer Science
University of Newcastle
Australia
Email: andrew.fleming@newcastle.edu.au

Sumeet S. Aphale
Centre for Applied Dynamics Research
School of Engineering
University of Aberdeen
UK
Email: s.aphale@abdn.ac.uk

Positive Velocity and Position Feedback (PVPF) is a widely used control scheme in lightly damped resonant systems with collocated sensor actuator pairs. The popularity of PVPF is due to the ability to achieve a chosen damping ratio by repositioning the poles of the system. The addition of a tracking controller, to reduce the effects of inherent nonlinearities, causes the poles to deviate from the intended location and can be a detriment to the damping achieved. By designing the PVPF and tracking controllers simultaneously, the optimal damping and tracking can be achieved. Simulations show full damping of the first resonance mode and significantly higher bandwidth than that achieved using the traditional PVPF design method, allowing for high speed scanning with accurate tracking. Experimental results are also provided to verify performance in implementation.

1 Introduction

Highly resonant systems suffer from harmonic excitation which can lead to performance degradation and even structural damage. Previous research suggests a myriad of options to manage the behaviour of such systems. In this work, we consider a nanopositioning platform. The performance of nanopositioners is limited by two features of their construction: firstly, nanopositioners have a low resonance frequency, and secondly, the piezoelectric actuators exhibit nonlinear behaviour.

In open-loop operation, the speed at which a flexure-based piezo-actuated nanopositioner can accurately trace a raster scan input is limited to approximately one-hundredth of its dominant resonance frequency [1]. However, there is a growing need for systems capable of high scanning speeds [2,3]. In order to combat the effect of the low resonance frequency, a damping controller is used. Integral Resonant Control (IRC) [4] and Integral Force Feedback (IFF) [5] are simple, robust and easy to implement damping controllers which utilise similar control laws. The development of Optimal Integral Force Feedback (OIFF) has made IFF identical to IRC from an analytical standpoint [6]. Though IRC has more scope for improvement, due to the arbitrary assignment of its feedthrough term, both controllers are limited in terms of achievable closed-loop poles. Resonant Control [7], Positive Position Feedback (PPF) [8] and Positive Velocity and Position Feedback (PVPF) [9] have been previously compared for suitability in nanopositioning applications using noise rejection as the performance criteria [7]. In that case PVPF was found to be the preferred choice. PVPF is also capable of arbitrary pole placement, whereas PPF is not. This allows full control over the closed-loop performance characteristics of the nanopositioner. For this reason, PVPF will be used in this work.

The nonlinear behaviour observed in the operation of piezo-actuated nanopositioners comes primarily from hysteresis. This can result in significant positioning errors over the full scan range and necessitates additional methods of control to counteract the effects. Various methods have been reported in previous research, such as charge actuation [10,11], the augmentation of linear control schemes with

Journal of Dynamic Systems, Measurement and Control. Received December 18, 2014;
Accepted manuscript posted June 2, 2015. doi:10.1115/1.4030723

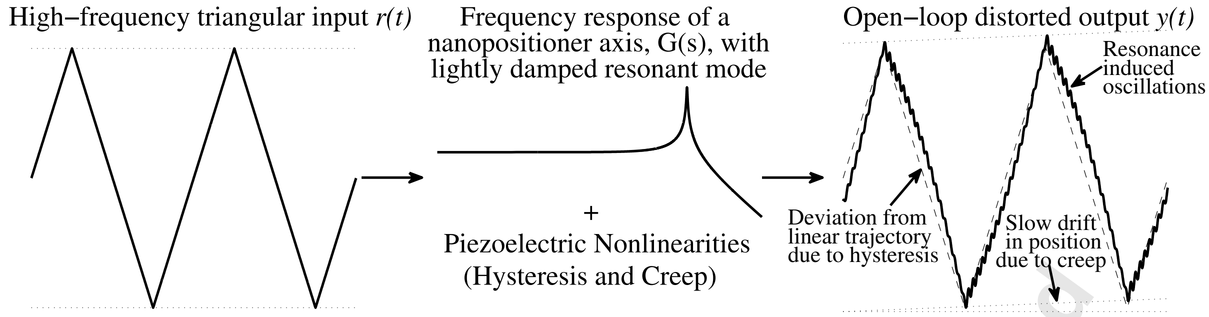

Fig. 1. Interaction of input harmonics and plant dynamics. On the left is a typical input for nanopositioning systems, a high frequency triangular waveform. The typical magnitude response of a lightly damped resonant system is presented in the centre. On the right is the resultant distorted output showing the effects of the lightly damped resonance, creep and hysteresis. Note, the effects have been exaggerated for illustrative purposes.

nonlinear damping [12, 13], and fuzzy control [14]. However, in nanopositioning, the reduction of positioning errors due to the inherent nonlinearities of piezoactuators is typically achieved through reference tracking [15]. Though linear control cannot fully negate nonlinear behaviour, previous works, where integral tracking is used, show a significant reduction in positioning errors [7, 9, 16].

In the previously cited works, the controllers are designed sequentially, i.e. the damping controller is designed using an appropriate method, the tracking controller is then added and the gain tuned by trial-and-error. The tracking controller causes a change in the location of the damped poles, thereby altering the damping characteristics of the system. By designing both the damping and tracking controllers simultaneously, the desired damping and tracking performance can be achieved. In this work, a method is provided for the simultaneous design of the damping and tracking controllers in order to achieve a flat band response.

Whilst H_2/H_∞ optimal control strategies can be employed to achieve the desired damping and tracking characteristics [17], there is a need for low-order, experimentally tunable controllers. In nanopositioning applications, variations in system dynamics, due to modelling uncertainties and loading of the nanopositioning platform, can cause performance degradation. Robustifying H_2/H_∞ designs improve performance in such circumstances. However, low-order controllers, including PVPF, are needed as the tracking controller gain can easily be fine-tuned to optimise performance in the presence of uncertainties.

The paper is structured as follows, Section II provides an overview of PVPF before presenting a method of deriving optimal controller parameters. In Section III, optimal controller parameters are derived for two axes of a nanopositioning platform. Simulations are provided to validate the theoretical work in Section II, assuring the objective of a flat band response is met. Section IV presents experimental results, showing the effectiveness of the proposed controller design in implementation. Section V concludes the paper.

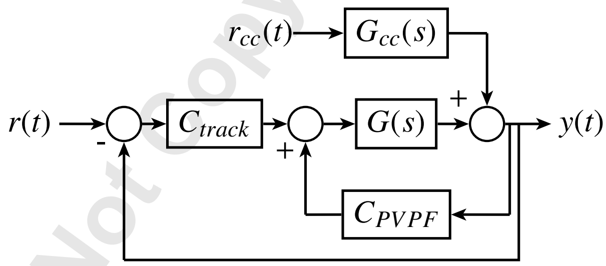

Fig. 2. Block diagram of the damped and tracked PVPF scheme, where $G(s)$ is the plant, $G_{cc}(s)$ is the FRF measuring the cross-coupling between the axes, $C_{PVPF}(s)$ is the PVPF damping controller, and $C_{track}(s)$ is the tracking controller.

2 Control Strategy

The effects of a nanopositioners resonance mode and nonlinear behaviours are depicted in Fig. 1. Applying a triangular input wave, the measured position is distorted by oscillations near the resonance frequency, deviation from the linear trajectory (hysteresis), and a drift in position (creep). In order to reduce the positioning error, closed-loop control is implemented, incorporating both damping (to reduce high-frequency distortions due to resonance-induced vibrations) and tracking (to reduce the positioning errors introduced by the piezoelectric nonlinearities) [15]. A closed-loop implementation, using a PVPF damping controller and integral tracking contoller, is shown in Fig. 2.

Positive Velocity and Position Feedback (PVPF) was introduced as an extension of the PPF controller. The addition of the velocity term allows arbitrary pole placement in the complex plane. It has been shown to be an effective vibration damping controller in nanopositioning applications [7, 9, 18]. In the following subsections, a brief overview of the traditional PVPF will be presented followed by a novel method of simultaneously placing the poles of the damping controller (PVPF-based) and the tracking controller (integral control). The main benefit of the proposed simultaneous pole-placement technique is the significant increase in closed-loop positioning bandwidth.

Journal of Dynamic Systems, Measurement and Control. Received December 18, 2014;
Accepted manuscript posted June 2, 2015. doi:10.1115/1.4030723

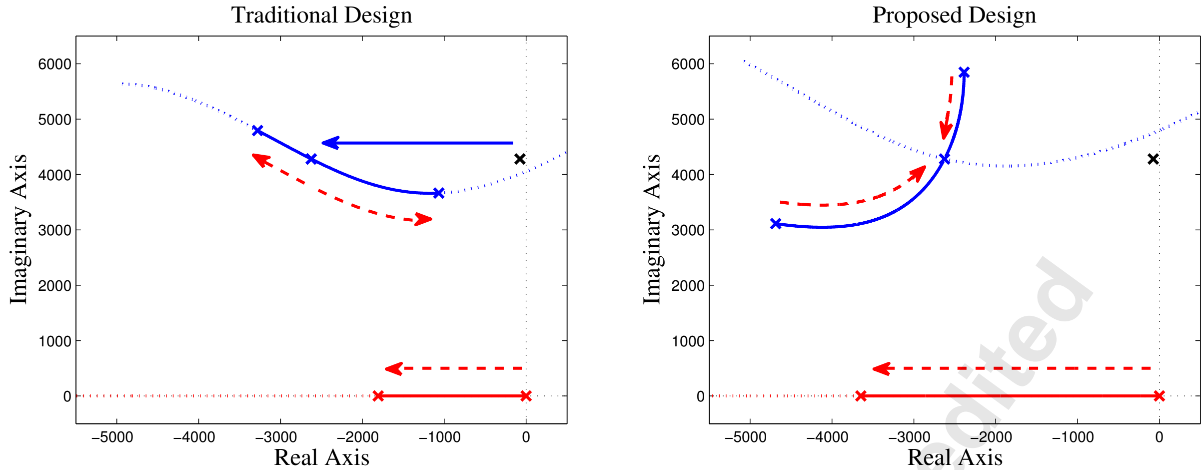

Fig. 3. Root loci of the tracking loop for the traditional controller design and the proposed controller design for the positive imaginary axis only. The black crosses are undamped poles of the open-loop system, blue crosses are the damped poles of the closed-loop system, and the red cross depicts the pole introduced by the tracking controller. The blue solid (—) arrow indicates the effect of the damping controller, and the red dashed (- - -) arrow the effect of the tracking controller. In the traditional PVPF design, the tracking controller displaces the complex poles from the intended location as the tracking gain is increased. The proposed control design places the damped poles at different strategic locations such that when the desired tracking gain is reached, the PVPF-induced poles converge on the desired (damped) location.

2.1 Traditional PVPF design

In nanopositioning, the control action is aimed at damping the dominant resonance mode. Therefore, the frequency response of a nanopositioner measured from the applied voltage to the displacement can be represented by a second-order model which has transfer function

$$G(s) = \frac{\sigma^2}{s^2 + 2\zeta\omega_n s + \omega_n^2}, \tag{1}$$

where ζ is the damping ratio, ω_n is the natural frequency, and σ^2 is chosen to match the DC gain of the plant. A model of this form has been derived from the mechanical configuration of the nanopositioning platform in [19]. Nonlinearities are not considered in the modelling of the plant as reference tracking reduces the effects. The PVPF controller, shown in Fig. 2 as C_{PVPF}, has transfer function

$$C_{PVPF}(s) = \frac{\Gamma_2 s + \Gamma_1}{s^2 + 2\gamma\omega_c s + \omega_c^2}. \tag{2}$$

An integrator is used as a tracking controller, C_{track} in Fig. 2, given by

$$C_{track}(s) = \frac{k_t}{s}. \tag{3}$$

The PVPF control scheme is designed by first choosing a damping controller to place the poles of the closed-loop system at a specified location. Typically, this location is chosen by reducing the real component of the open-loop poles by a sufficiently large amount, such that the damping ratio is increased whilst maintaining the damped natural frequency. A tracking controller is then added and the gain is tuned to obtain the desired response. However, it has been shown that there is a relationship between the damping and tracking controllers and system stability [20]. For this reason, the damping and tracking controllers will be designed simultaneously, i.e. only the damped and tracked system will be considered.

Denoting the numerator of a transfer function G^{num}, and the denominator G^{den}, such that $G = G^{num}/G^{den}$, the damped and tracked closed-loop system, measured from input, $r(t)$, to output, $y(t)$, is given by

$$\begin{aligned} G_{cl}^{num}(s) &= k_t\sigma^2(s^2 + 2\gamma\omega_c + \omega_c^2) \\ G_{cl}^{den}(s) &= s^5 + (2\zeta\omega_n + 2\gamma\omega_c)s^4 + (2\zeta\omega_n 2\gamma\omega_c + \omega_n^2 + \omega_c^2)s^3 \\ &\quad + (2\zeta\omega_n\omega_c^2 + 2\gamma\omega_c\omega_n^2 - \sigma^2\Gamma_2 + k_t\sigma^2)s^2 \\ &\quad + (\omega_n^2\omega_c^2 - \sigma^2\Gamma_1 + k_t\sigma^2 2\gamma\omega_c)s + k_t\sigma^2\omega_c^2 \end{aligned} \tag{4}$$

This is used in the derivation of the proposed controller parameters. The optimisation process applies a change of variables to aid computation. Equation (4) is used in reverting to the original variable set.

2.2 Simultaneous Damping and Tracking via Selective Pole Placement

The traditional PVPF control scheme places the poles of the damped system at a specific location. As the tracking controller is implemented and the gain increased, the poles diverge from the chosen location. In this work, the opposite is desired. The damping controller places the poles at two distinct locations. As the tracking controller gain is increased to the optimal amount, the complex poles converge

Journal of Dynamic Systems, Measurement and Control. Received December 18, 2014;
Accepted manuscript posted June 2, 2015. doi:10.1115/1.4030723

at the desired location, see Fig. 3. In order to achieve this, the pole placement is specified for the damped and tracked closed-loop system. Then, the controller parameters for both the damping and tracking controllers are derived simultaneously. In contrast to the traditional PVPF approach, this method ensures the desired damping ratio is achieved in the damped and tracked closed-loop system. The damped and tracked system has the following characteristic equation

$$P(s) = (s+\omega_p)(s^2 + 2\psi\omega_d s + \omega_d^2)^2. \tag{5}$$

where ω_p is the real pole introduced by the tracking controller, ω_d is the damped natural frequency of the open-loop system, for lightly damped systems this is approximately equal to ω_n, and ψ is the desired damping ratio. Equating this with the denominator in Eq. (4) gives the equivalent damped and tracked closed-loop system in terms of the desired system variables. This derivation makes the assumption that the damping ratio, ζ, is sufficiently small and can be neglected.

$$\begin{aligned}
G_{cl}^{num}(s) &= \frac{\omega_d^4\omega_p(s^2 + (4\psi\omega_d + \omega_p)s + (5\psi\omega_d^2 + \omega_d^2 + 4\psi\omega_d\omega_p))}{5\psi\omega_d^2 + \omega_d^2 + 4\psi\omega_d\omega_p} \\
G_{cl}^{den}(s) &= s^5 + (4\psi\omega_d + \omega_p)s^4 + (4\psi^2\omega_d^2 + 2\omega_d^2 + 4\psi\omega_d\omega_p)s^3 \\
&+ (4\psi\omega_d^3 + 4\psi^2\omega_d^2\omega_p + 2\omega_d^2\omega_p)s^2 + (\omega_d^4 + 4\psi\omega_d^3\omega_p)s + \omega_d^4\omega_p.
\end{aligned} \tag{6}$$

The aim is to choose ψ and ω_d to achieve a desired amount of damping, and find the ω_p which will give a flat-band response, i.e. $|G_{cl}(j\omega)|_{dB} \leq 0 \ \forall \ \omega \in \mathbb{R}$. The controller parameters are found by equating the denominator terms of Eq. (4) with the desired characteristic equation. For $|G_{cl}(j\omega)|_{dB} \leq 0$, the following is true

$$\begin{gathered}
|G_{cl}(j\omega)| \leq 1 \\
\frac{\left|G_{cl}^{num}(j\omega)\right|}{\left|G_{cl}^{den}(j\omega)\right|} \leq 1 \\
\left|G_{cl}^{num}(j\omega)\right|^2 \leq \left|G_{cl}^{den}(j\omega)\right|^2 \\
\left|G_{cl}^{den}(j\omega)\right|^2 - \left|G_{cl}^{num}(j\omega)\right|^2 \geq 0.
\end{gathered}$$

Substituting the numerator and denominator of the closed-loop transfer function, Eq. (6), gives the following:

$$\begin{aligned}
&\big(\omega^{10} + (8\psi^2\omega_d^2 + \omega_p^2 - 4\omega_d^2)\omega^8 \\
&+ (-16\psi^2\omega_d^4 + 8\psi^2\omega_d^2\omega_p^2 - 4\omega_d^2\omega_p^2 + 6\omega_d^4 + 16\psi^4\omega_d^4)\omega^6 \\
&+ (6\omega_d^4\omega_p^2 + 8\psi^2\omega_d^6 - 16\psi^2\omega_d^4\omega_p^2 + 16\psi^4\omega_d^4\omega_p^2 - 4\omega_d^6)\omega^4 \\
&+ (\omega_d^8 + 8\psi^2\omega_d^6\omega_p^2 - 4\omega_d^6\omega_p^2)\omega^2 + \omega_d^8\omega_p^2\big) \\
&- \left(\frac{\omega_d^4\omega_p}{5\psi\omega_d^2 + \omega_d^2 + 4\psi\omega_d\omega_p}\right)^2 \big(\omega^4 + (6\psi^2\omega_d^2 - 2\omega_d^2 + \omega_p^2)\omega^2 \\
&+ (25\psi^4\omega_d^4 + \omega_d^4 + 16\psi^2\omega_d^2\omega_p^2 + 10\psi^2\omega_d^4 + 40\psi^3\omega_d^3\omega_p + 8\psi\omega_d^3\omega_p)\big) \\
&\geq 0.
\end{aligned} \tag{7}$$

As the system is type 1, the ω^0 terms of the numerator and denominator of the transfer function are equal. Thus, the ω^0 terms in Eq. 7 are equal. Subtracting the ω^0 terms and dividing by ω^2 gives

$$\begin{aligned}
&\big(\omega^8 + (8\psi^2\omega_d^2 + \omega_p^2 - 4\omega_d^2)\omega^6 \\
&+ (-16\psi^2\omega_d^4 + 8\psi^2\omega_d^2\omega_p^2 - 4\omega_d^2\omega_p^2 + 6\omega_d^4 + 16\psi^4\omega_d^4)\omega^4 \\
&+ (6\omega_d^4\omega_p^2 + 8\psi^2\omega_d^6 - 16\psi^2\omega_d^4\omega_p^2 + 16\psi^4\omega_d^4\omega_p^2 - 4\omega_d^6)\omega^2 \\
&+ (\omega_d^8 + 8\psi^2\omega_d^6\omega_p^2 - 4\omega_d^6\omega_p^2)\big) \\
&- \left(\frac{\omega_d^4\omega_p}{5\psi\omega_d^2 + \omega_d^2 + 4\psi\omega_d\omega_p}\right)^2 \big(\omega^2 + (6\psi^2\omega_d^2 - 2\omega_d^2 + \omega_p^2)\big) \geq 0.
\end{aligned} \tag{8}$$

A flat-band response is achieved when the above equation is approximately equal to zero over a defined range of frequencies.

2.2.1 Complex Pole Placement

In traditional PVPF design, the location of the complex poles is chosen by shifting the open-loop poles of the system by an arbitrary amount into the left-half plane, typically in the region of 1000 units, i.e. the real component of the open-loop poles is reduced by 1000. The complex poles in the proposed controller are chosen by selecting a desired damping ratio to achieve a predetermined amount of damping.

For a second-order system with normalized input/output gain, the transfer function is

$$G(s) = \frac{\omega_n^2}{s^2 + 2\zeta\omega_n s + \omega_n^2}, \tag{9}$$

and has magnitude response

$$|G(j\omega)| = \frac{\omega_n^2}{\sqrt{\omega^4 + (4\zeta^2\omega_n^2 - 2\omega_n^2)\omega^2 + \omega_n^4}}. \tag{10}$$

For a given bandwidth of $\pm x$ dB, $|G(j\omega)|$ should not pass through the upper bound on bandwidth, i.e.

$$|G(j\omega)| \leq 10^{\frac{x}{20}} : \forall\omega \in \mathbb{R} \tag{11}$$

Substituting Eq. (10) and rearranging gives

$$\omega^4 + (4\zeta^2\omega_n^2 - 2\omega_n^2)\omega^2 + \omega_n^4 - \omega_n^4 \times 10^{\frac{-x}{10}} \geq 0. \tag{12}$$

The roots of Eq. (12) give the frequencies at which $|G(j\omega)|$ crosses x dB. If Eq. (12) has two real and distinct roots, $|G(j\omega)| > x$ dB for some ω, if the roots are real and equal, $|G(j\omega)| = x$ dB for only one value of ω, and if the roots are complex $|G(j\omega)| < x\ dB\ \forall\omega$. It is obvious that real and equal roots will provide maximum bandwidth. In this case, the

Journal of Dynamic Systems, Measurement and Control. Received December 18, 2014;
Accepted manuscript posted June 2, 2015. doi:10.1115/1.4030723

discriminant of Eq. (12) is equal to zero, i.e.

$$\begin{aligned}(4\zeta^2\omega_n^2 - 2\omega_n^2)^2 + 4\omega_n^4 \times 10^{\frac{-x}{10}} &= 0\\ 4\omega_n^4(4\zeta^4 - 4\zeta^2 + 10^{\frac{-x}{10}}) &= 0\\ \Rightarrow \zeta &= \sqrt{\frac{4 \pm \sqrt{16 - 16 \times 10^{\frac{-x}{10}}}}{8}}\end{aligned} \tag{13}$$

Pole placement such that the damping ratio is that given by Eq. (13) will therefore provide maximum $\pm x$ dB bandwidth relative to the DC gain of a second-order system. For a ± 1 dB bandwidth, as required in nanopositioning, this gives the damping ratio, $\zeta = 0.5227$.

2.2.2 Real Pole Placement

The real pole is chosen to provide a flat-band response over a given frequency range. Care must be taken when choosing the upper limit of the frequency range as an incorrect choice can result in resonance. Through simulation, it is found that the natural frequency of the plant is sufficient to achieve a flat-band response.

For fixed complex poles, represented by ψ, ω_d, Eq. (8) can be defined as a function of the real pole, ω_p, and the frequency, ω, as $H(\omega_p, \omega)$. We choose ω_p such that the following equation is minimized over the bandwidth of interest, i.e. $\omega \in [0, \omega_n]$,

$$\min \left| \sum_{\omega=0}^{\omega_n} H(\omega_p, \omega) \right|. \tag{14}$$

This gives the closed loop frequency response, $G_{cl}(j\omega)$, which is closest to unity gain over the chosen frequency range. Note that, due to the fixed location of the complex poles in the damped and tracked closed-loop system, the choice of real pole affects not only the tracking controller gain but also the parameters of the PVPF damping controller. This differs from the traditional approach in that the choice of real pole does not alter the damping ratio of the complex poles in the closed-loop system.

2.2.3 Controller Synthesis

The controller parameters are derived using a method that is similar to that used in traditional PVPF design. The only differences being the inclusion of the tracking gain, k_t, and the adoption of a different set of variables to ensure the desired closed-loop poles are achieved.

With the three system variables, ω_p, ω_d, ψ, defined numerically, the characteristic equation of the system will be of the form

$$s^5 + K_4 s^4 + K_3 s^3 + K_2 s^2 + K_1 s + K_0. \tag{15}$$

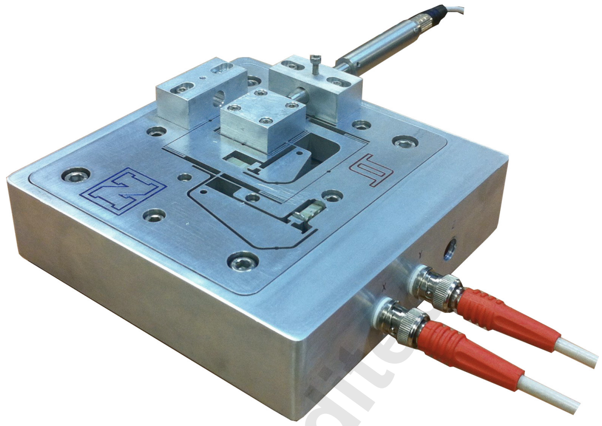

Fig. 4. A two-axis 40 μm serial kinematic nanopositioner designed at the EasyLab, University of Nevada, Reno

Equating this with Eq. (4) gives the controller parameters as

$$\begin{aligned}2\gamma\omega_c &= K_4 - 2\zeta\omega_n\\ \omega_c^2 &= K_3 - \omega_n^2 - 2\zeta\omega_n 2\gamma\omega_c\\ k_t &= K_0/(\sigma^2\omega_c^2)\\ \Gamma_2 &= -(K_2 - 2\zeta\omega_n\omega_c^2 - 2\gamma\omega_c\omega_n^2 - k_t\sigma^2)/\sigma^2\\ \Gamma_1 &= -(K_1 - \omega_c^2\omega_n^2 - 2\gamma\omega_c k_t\sigma^2)/\sigma^2\end{aligned} \tag{16}$$

In the following section, the developed control strategy is applied to a 2×2 nanopositioning platform. The system is modelled on the measured frequency response, optimal pole placement is found using Eq. (14), and the optimal controller parameters are derived from Eqs. (2) and (3).

3 Experimental Setup and Simulations

The performance of the proposed controller is evaluated on a two-axis serial kinematic nanopositioner, pictured in Fig. 4.

3.1 Experimental Setup

The nanopositioner was designed and constructed at the EasyLab, University of Nevada, Reno. The stage is driven by two 10 mm 200 V piezoelectric stack actuators that provide a range of 40 μm in each axis. The position is measured by a Microsense 6810 capacitive sensor and 6504-01 probe with a sensitivity of 2.5 μm/V. The stage is driven by two PiezoDrive PDL200 voltage amplifiers with a gain of 20. The control algorithm was implemented using the dSPACE DS1103 rapid prototyping system consisting of 16-bit A/D input channels and 16-bit D/A output channels operating in parallel at a sampling rate of 20 kHz. All the transfer functions were recorded using a HP35670A Dynamic Signal Analyzer.

The simulations are performed using both a second-order model, as in Eq. (1), and a full `frd`-model based on the aforementioned nanopositioning system. The coupled axes

Journal of Dynamic Systems, Measurement and Control. Received December 18, 2014;
Accepted manuscript posted June 2, 2015. doi:10.1115/1.4030723

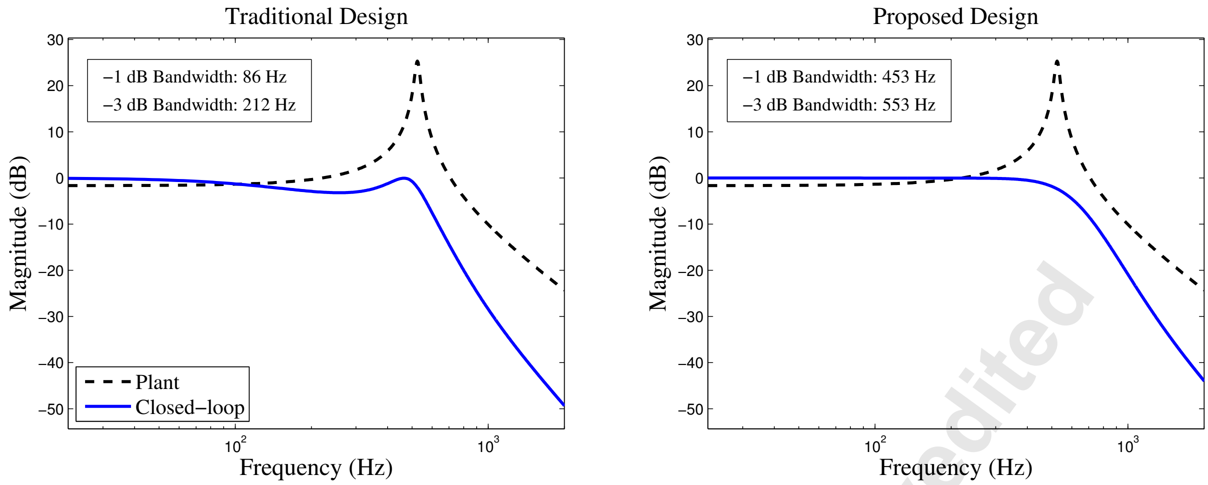

Fig. 5. Simulated magnitude response of the closed-loop, damped and tracked system for both the traditional PVPF design and the proposed technique that incorporates simultaneously designed damping and tracking controllers optimized via selective pole-placement.

are not modelled, therefore, only the `frd` results are provided for those axes. The x- and y-axis models are derived from the measured frequency response using the discrete time system identification algorithm described in [21]. The continuous time model is then found by bilinear transform giving

$$G_{xx}(s) = \frac{8.9793\times10^6}{s^2+147s+1.0881\times10^7} \tag{17}$$

$$G_{yy}(s) = \frac{1.3888\times10^7}{s^2+148s+1.8325\times10^7} \tag{18}$$

3.2 *X*-axis Controller

To validate the performance of the proposed controller design, both a traditional PVPF control scheme and the proposed control scheme are designed and simulated using the second-order model of the x-axis to compare achievable bandwidth.

3.2.1 Traditional PVPF Design

The traditional PVPF controller is designed using the method laid out in [7] and [9]. In these works, the closed-loop damping ratios achieved are $\zeta = 0.356$ and $\zeta = 0.371$ respectively. In order to achieve similar performance, the poles are moved 1350 units into the left half plane, i.e. the closed-loop poles are placed at $-1423.5\pm i3297.8$. This gives a closed loop damping ratio of $\zeta = 0.396$. The tracking controller gain is found via trial-and-error, such that the magnitude response does not exceed 0 dB. The traditional PVPF and tracking controllers are

$$C_{PVPF,x}(s) = \frac{-1096s+8.379\times10^6}{s^2+5547s+2.221\times10^7} \tag{19}$$

$$C_{track,x}(s) = \frac{700}{s}. \tag{20}$$

3.2.2 Proposed Controller Design

As derived in Section 2.2.1, a damping ratio of 0.5227 is desired. This provides a frequency response with magnitude no greater than 1 dB for a second-order system. As the damped system is fourth order, the frequency response will have a maximum resonance peak of no more than 2 dB. Setting the damping ratio, $\psi = 0.5227$, and damped natural frequncy $\omega_d = \omega_n = 3298.6$, the complex poles of the desired closed-loop transfer function are $-2022.5\pm i3298.6$. From Eq. (14), the real pole, ω_p, which gives a flat band response is found to be -2809.2. This gives the desired characteristic equation as

$$s^5+1.0899\times10^4s^4+6.9031\times10^7s^3+2.5120\times10^{11}s^2 +5.6439\times10^{14}s+6.2967\times10^{17}. \tag{21}$$

Using Eq. (16) the controller parameters are calculated. The simultaneously designed controllers are denoted by $C_{sPVPF}(s)$ and $C_{strack}(s)$, and given by

$$C_{sPVPF,x}(s) = \frac{-1.278\times10^4s+1.902\times10^7}{s^2+1.075\times10^4s+5.657\times10^7} \tag{22}$$

$$C_{strack,x}(s) = \frac{1240}{s}. \tag{23}$$

The simulated magnitude response is presented in Fig. 5. It is observed that the proposed controller provides significantly higher bandwidth. For this reason, the proposed controller design is applied to the y-axis and simulated for the full 2×2 model of the plant.

3.3 *Y*-axis Controller

Using the same method as for the x-axis design, the complex poles are set to $-2624.7\pm i4280.8$, the real pole is

Journal of Dynamic Systems, Measurement and Control. Received December 18, 2014;
Accepted manuscript posted June 2, 2015. doi:10.1115/1.4030723

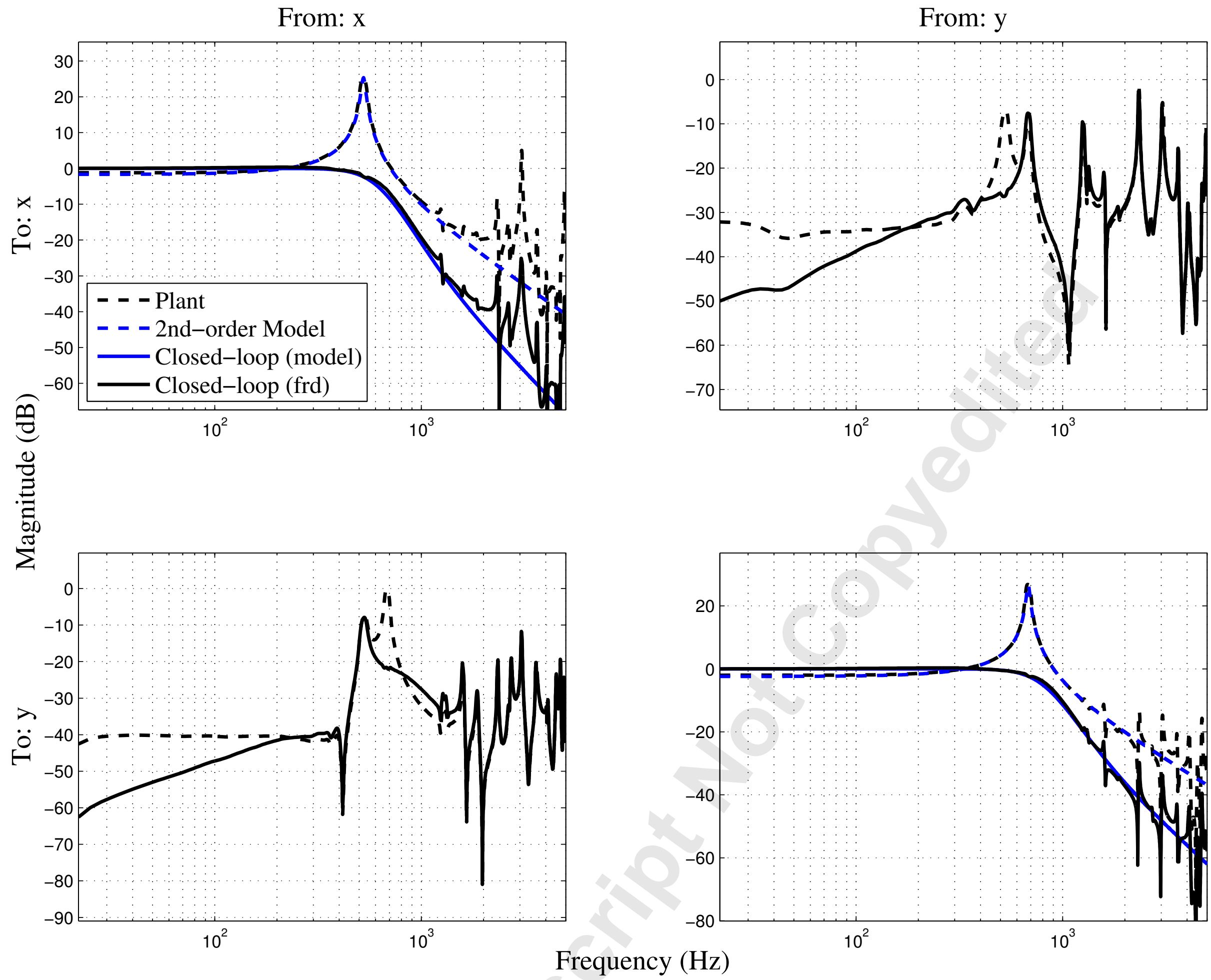

Fig. 6. Measured magnitude response of the nanopositioning platform (blue) and the derived second-order model (black), both denoted by dashed (—) lines. Higher-order models needed to capture the cross-coupling dynamics are not required for the control design and are not derived. Simulated closed-loop magnitude responses of the nanopositioning platform with PVPF controller are provided for both the second-order model and the full `frd`-model. As can be seen in the x- (top left) and y-axis (bottom right) FRFs, the response is very similar in the frequency range of interest. The higher order modes have little effect on the response below the first resonance mode.

found to be -3648.3, giving the desired characteristic equation

$$s^5 + 1.4147\times10^4 s^4 + 1.1629\times10^8 s^3 + 5.4922\times10^{11} s^2 + 1.6015\times10^{15} s + 2.3194\times10^{18}. \tag{24}$$

Eq. (16) gives the controllers

$$C_{sPVPF,y}(s) = \frac{-1.831\times10^4 s + 3.559\times10^7}{s^2 + 1.4\times10^4 s + 9.589\times10^7} \tag{25}$$

$$C_{strack,y}(s) = \frac{1742}{s}. \tag{26}$$

The simulated magnitude response of the nanopositioning platform is provided in Fig. 6.

4 Experimental Results and Discussion

In this section, experimental results are provided for the nanopositioning platform, as described in Section 3.1. Results are given in the form of measured closed-loop magnitude responses, of the 2×2 system, and the measured position of both axes tracing a raster scan pattern.

4.1 Frequency Domain Results

The measured closed-loop response is shown in Fig. 7. The measured bandwidth is given in Table 1. Here bandwidth is defined as the range of frequencies for which the frequency response is between ±1 dB. This is done for two reasons. First, the traditional -3 dB bandwidth results in a loss of signal strength of approximately 30%, as such, it is not suitable for use in precise positioning applications [20]. Second, both upper and lower limits are required in defining bandwidth as an exceedingly high response can have an equally detrimental effect on performance. The ±3 dB bandwidth is also provided.

Journal of Dynamic Systems, Measurement and Control. Received December 18, 2014;
Accepted manuscript posted June 2, 2015. doi:10.1115/1.4030723

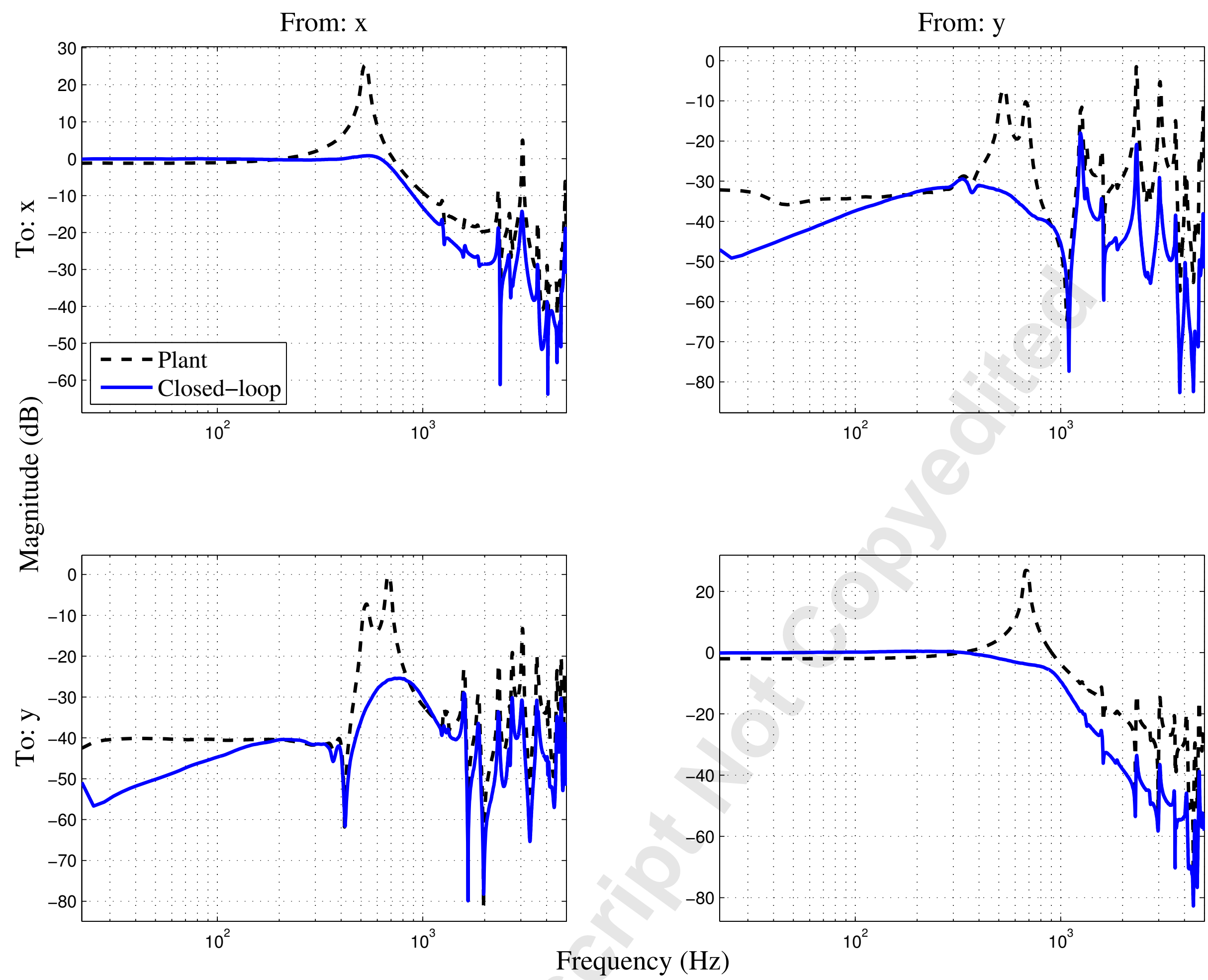

Fig. 7. Experimentally measured open- and closed-loop magnitude response of the nanopositioning platform with PVPF and tracking controllers.

The closed-loop implentation of the control scheme is seen to be stable. The measured bandwidth of both axes is similar to that found in simulation. The effects of the higher order dynamics are lessened due to the increased roll-off rate at high frequencies. In the coupled axes it is observed that the response is reduced at low frequencies. Additionally, it is noted that the dominant resonance mode of both the x- and y-axes are damped.

Table 1. Experimental Results

	x-axis	y-axis
Resonance Frequency (Hz)	525	681
Bandwidth ±1 dB (Hz)	428	656
Bandwidth ±3 dB (Hz)	593	715
Max. Error (μm)	0.0165	0.2580
RMS Error (μm)	0.0048	0.0190

4.2 Time Domain Results

Typical positioning performance of nanopositioners is tested by forcing the nanopositioner to trace a raster pattern [1, 15]. A raster pattern is generated by a combination of a slow staircase or ramp input along one axis and a relatively high-frequency triangle wave input along the other.

The closed-loop response is tested using a ±1.25 μm, 20 Hz triangle wave as the x-axis input and a 10 Hz repeating step function, increasing in increments of 0.25 μm, within the range ±1.25 μm , as the y-axis input.

The experimental data displays tracking of the reference which closely matches that predicted by simulation. The x-axis response shows accurate tracking of the reference, with an RMS error of 0.48%. The measured RMS error of the y-axis response is larger at 1.9%. This is somewhat skewed by the considerable error incurred due to lag at the step. In practice, this is largely inconsequential as it can be omitted from the data used to formulate output in the primary application of nanopositioning, imaging.

The scan results shown in Figs. 8 and 9 clearly show that the proposed control technique has successfully suppressed the resonance-induced positioning errors. The straight-line trajectories of the raster also show that the proposed control strategy reduced the positioning errors introduced by the in-

Journal of Dynamic Systems, Measurement and Control. Received December 18, 2014;
Accepted manuscript posted June 2, 2015. doi:10.1115/1.4030723

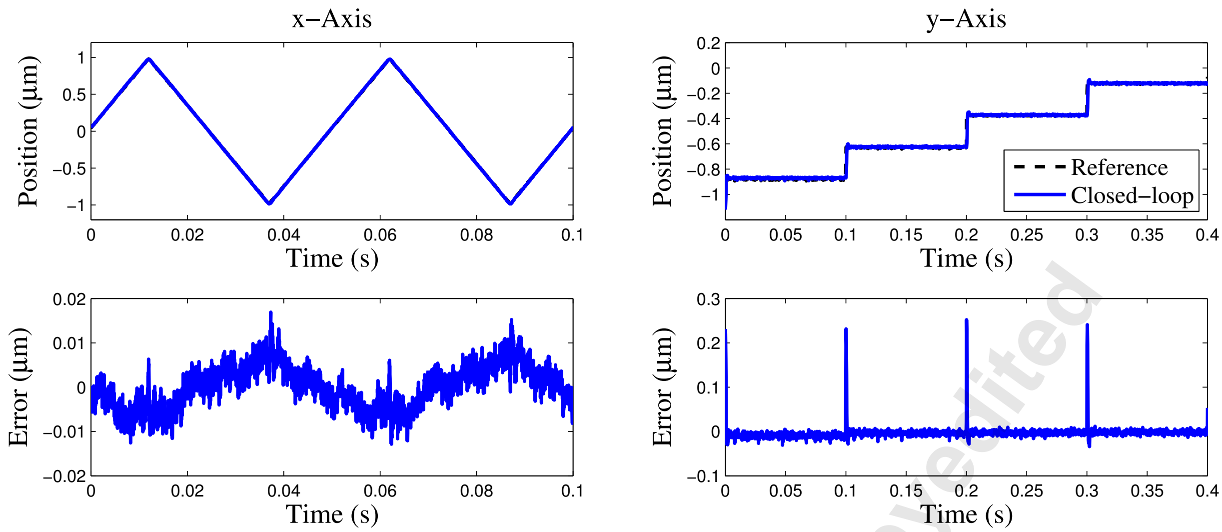

Fig. 8. Plot of the phase-corrected x- and y-axis output (top row) and the error relative to the input (bottom row)

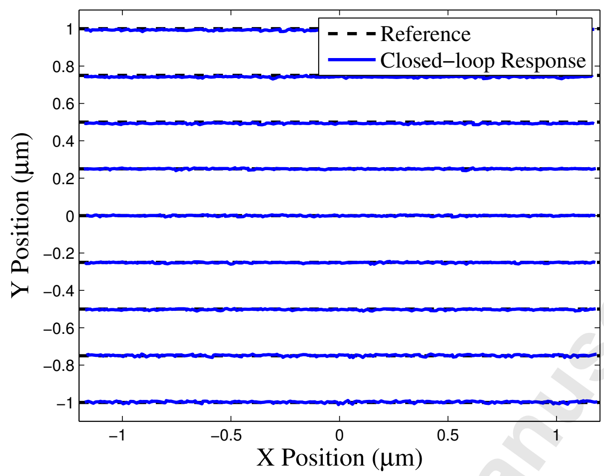

Fig. 9. Raster scan where the x-axis input is a 20 Hz triangle wave with amplitude ± 1.25 μm, and the y-axis input is 10 Hz stepping function which increases by 0.25 μm each period and the step coincides with the lowest point of the x-axis trajectory. The phase-lag-induced artifacts present in the full scan during the transition between each consecutive increment of the stepping function have been removed, leaving only the usable scan lines.

herent nonlinearities (hysteresis and creep) present in piezoelectric actuators.

5 Conclusion

This paper presents a method for simultaneously optimizing the parameters of a PVPF damping controller and an integral tracking controller for high-precision positioning applications. The model-based simulations show a significantly greater bandwidth than the traditional PVPF implementation and flat band response at low frequencies, perfectly suited to high-speed scanning. The experimental results exhibit the effect of the system's higher order dynamics but confirm the results of the simulations, maintaining a largely flat response and similarly high bandwidth. This method, therefore, provides a cost-effective, easy to implement improvement of the positioning bandwidth of existing nanopositioners.

References

[1] Moheimani, S. O. R., 2008. "Invited review article: Accurate and fast nanopositioning with piezoelectric tube scanners: Emerging trends and future challenges". *Review of Scientific Instruments,* **7**(7).
[2] Ando, T., Kodera, N., Maruyama, D., Takai, E., Saito, K., and Toda, A., 2002. "A high-speed atomic force microscope for studying biological macromolecules in action". *Japanese Journal of Applied Physics,* **41**(7B), pp. 4851–4856.
[3] Tuma, T., Lygeros, J., Kartik, V., Sebastian, A., and Pantazi, A., 2012. "High-speed multiresolution scanning probe microscopy based on lissajous scan trajectories". *Nanotechnology,* **23**(18).
[4] Aphale, S. S., Fleming, A. J., and Moheimani, S. O. R., 2007. "Integral resonant control of collocated smart structures". *Smart Materials and Structures,* **16**, February, pp. 439 – 446.
[5] Preumont, A., de Marneffe, B., Deraemaeker, A., and Bossens, F., 2008. "The damping of a truss structure with a piezoelectric transducer". *Computers and Structures,* **86**, pp. 227 – 239.
[6] Teo, Y. R., Russell, D., Aphale, S. S., and Fleming, A. J., 2014. "Optimal integral force feedback and structured pi tracking control: Application for objective lens positioner". *Mechatronics, in Press*.
[7] Aphale, S. S., Bhikkaji, B., and Moheimani, S. R., 2008. "Minimizing scanning errors in piezoelectric stack-actuated nanopositioning platforms". *IEEE Transactions on Nanotechnology,* **7**(1), pp. 79–90.
[8] Fanson, J. L., and Caughey, T. K., 1990. "Positive posi-

Journal of Dynamic Systems, Measurement and Control. Received December 18, 2014;
Accepted manuscript posted June 2, 2015. doi:10.1115/1.4030723

tion feedback control for large space structures". *AIAA Journal,* **28**(4), pp. 717 – 724.

[9] Bhikkaji, B., Ratnam, M., Fleming, A. J., and Moheimani, S. O. R., 2007. "High-performance control of piezoelectric tube scanners". *IEEE Transactions on Control Systems Technology,* **15**(5), September, pp. 853 – 866.

[10] Newcomb, C., and Flinn, I., 1982. "Improving the linearity of piezoelectric ceramic actuators". *Electronics Letters,* **18**(11), pp. 442–444.

[11] Fleming, A. J., 2013. "Charge drive with active dc stabilization for linearization of piezoelectric hysteresis". *IEEE Transactions on Ultrasonics, Ferroelectrics and Frequency Control,* **60**(8), pp. 1630–1637.

[12] Kanestrom, R. K., and Egeland, O., 1994. "Nonlinear active vibration damping". *IEEE Transactions on Automatic Control,* **39**(9), pp. 1925–1928.

[13] Vagia, M., Eilsen, A. A., Gravdahl, J. T., and Pettersen, K. Y., 2013. "Design of a nonlinear damping control scheme for nanopositioning". In 2013 IEEE/ASME International Conference on Advanced Intelligent Mechatronics.

[14] Yu, G., Huang, J., and Chen, Y., 2009. "Optimal fuzzy control of piezoelectric systems based on hybrid taguchi method and particle swarm optimization". In Proc. of the IEEE International Conference on Systems, Man, and Cybernetics.

[15] Devasia, S., Eleftheriou, E., and Moheimani, S. O. R., 2007. "A survey of control issues in nanopositioning". *IEEE Transactions on Control Systems Technology,* **15**(4), July, pp. 689 – 703.

[16] Fleming, A. J., 2010. "Nanopositioning system with force feedback for high-performance tracking and vibration control". *IEEE/ASME Transactions on Mechatronics,* **15**(3), pp. 433–447.

[17] Sebastian, A., and Pantazi, A., 2012. "Nanopositioning with multiple sensors: A case study in data storage". *IEEE Transactions on Control Systems Technology,* **20**(2), pp. 382 – 394.

[18] Bazaei, A., Yong, Y. K., Moheimani, S. O. R., and Sebastian, A., 2012. "Tracking of triangular references using signal transformation for control of a novel afm scanner stage". *IEEE Transactions on Control Systems Technology,* **20**(2), pp. 453–464.

[19] Fleming, A. J., Aphale, S. S., and Moheimani, S. O. R., 2010. "A new method for robust damping and tracking control of scanning probe microscope positioning stages". *IEEE Transactions on Nanotechnology,* **9**(4), July, pp. 438 – 448.

[20] Namavar, M., Fleming, A. J., Aleyaasin, M., Nakkeeran, K., and Aphale, S. S., 2014. "An analytical approach to integral resonant control of second-order systems". *IEEE Transactions on Mechatronics,* **19**(2), pp. 651–659.

[21] McKelvey, T., Akcay, H., and Ljung, L., 1996. "Subspace based multivariable system identification from frequency response data". *IEEE Transactions on Automatic Control,* **41**(7), pp. 960–979.